JSAP Review
JSAP Rev. **2024**, 240212
https://doi.org/10.11470/jsaprev.240212

Tutorial Review

Wetting phenomena and design of liquid-repellent surfaces

Mizuki Tenjimbayashi

National Institute for Materials Science (NIMS), Tsukuba, Ibaraki 305-0044, Japan
E-mail: TENJIMBAYASHI.Mizuki@nims.go.jp

Wetting is ubiquitous in nature and contributes significantly to industrial processes. This commentary focuses on solid/fluid interaction, which summarizes the fundamentals of wetting phenomena (surface tension, droplet shape, capillary force, and wetting models), the design strategy for liquid-repellent interfaces (superhydrophobic/superoleophobic surfaces and liquid marble), and the associated cutting-edge applications. The relevant equations utilize only thermodynamics concepts taught in high school and are explained concisely such that even beginners can understand them sensibly. Additionally, typical examples are provided.

Received March 7, 2024; Accepted April 18, 2024
Translated from Oyo Buturi **93**, 519 (2024) DOI: https://doi.org/10.11470/oubutsu.93.9_519

1. Introduction

Consider the following scenario: You take a shower first thing in the morning. The steam fogs up the mirror, various droplets and puddles form on the bathroom floor, and your hair gets wet and clumps up. You foam up your shampoo and wash your hair, and then dry your body and apply moisturizing cream. Next, you prepare breakfast. You spread jam on bread and prepare fried eggs in a frying pan with oil. You make coffee through a filter. When you leave the house, it is raining outside. You enter your waterproof-coating car and drive to work. These daily actions can be explained by the interaction between solids and fluids, i.e., the wetting phenomenon. In fact, the wetting phenomenon dominates all the industrial fields that pertain to our lives, including the cosmetics, textile, food, chemical, automotive, and glass industries. Therefore, understanding the physics behind this phenomenon is crucial. Simple wetting experiments can be performed using only tap water. The topic of wetting has been investigated in academia for more than 200 years; consequently, classical theories have been established that explain wetting phenomena well despite their simplicity [1,2]. Therefore, many researchers explain wetting phenomena using classical theories of wetting.

Parallel with the establishment of wetting theory, materials and surface-modification technologies for controlling wettability has been developed. In the early 1900s, synthesis techniques for hydrophobic materials such as silicone and Teflon, as well as surface chemical-modification techniques were reported, and by the 1990s, the development of nanotechnology has enabled the realization of surfaces with extreme wettability, such as superhydrophobic and superhydrophilic surfaces [3,4]. The number of articles pertaining to superhydrophobicity has increased exponentially since 2000, and these articles report various hydrophobic/oleophobic processing techniques and materials, as well as application examples [5].

Herein, we first explain the basics of wetting phenomena (surface energy and capillary force). Next, we introduce the relationship between surface structure and wettability. Subsequently, we explain a method to design superhydrophobic/superoleophobic surfaces (materials) and their applications.

2. Wetting phenomena

2.1 Surface free energy

Surface free energy is the most fundamental element in understanding wetting phenomena. An example (although not in the strict sense) is provided herein to illustrate surface free energy to the readers (Fig. 1A). Imagine children holding hands and forming a line. The child in the middle is happy because he/she is holding hands with the adjacent children. However, the child at the edge is only holding hands with the adjacent child with one hand; thus, he/she is not happy. The closer the friendship between the children, the greater is the difference in mood between the children in the middle and at the edges. This inequality can be eliminated by having the children at the edges holding hands with each other and forming a circle.

A similar phenomenon occurs at the molecular scale (Fig. 1B). Water droplets are formed by the accumulation of water molecules; however, adjacent water molecules in the interior of the droplet are bonded to each other. Meanwhile, water molecules on the surface of the droplet have no other water molecules at the air side (in fact, they exist as water vapor); thus, an energy difference occurs with the molecules in the interior of the droplet. This is the surface free energy (typically denoted as γ). In reference to Fig. 1B, the spherical shape of the water droplet is caused by the minimization of the contact area with the air to reduce the surface free energy and achieve an energetically stable state. However, unlike the case of people holding hands, when the droplet becomes spherical, the interface with the air cannot be eliminated, and the existence of a surface continuously creates an energy difference with the interior molecules. In other words, the surface free energy (expressed in units of J/m^2) is the energy per unit area that increases with the droplet surface area.

The magnitude of the surface free energy is determined by the interaction strength between molecules (analogous to the closeness in friendship in the human example) (in fact, the exposed surface area of the molecules is a contributing factor). For example, as summarized in Fig. 1C, nonpolar liquids such as hexane have a relatively low surface free energy owing to intermolecular forces being the only van der Waals interaction. Glycerol and water have high surface free energies owing to the presence of both intermolecular forces and hydrogen bonds. Liquid metals such as mercury have a surface free energy that is one order of magnitude higher than those of other liquids due to metallic bonds. Consequently, mercury droplets tend to form a sphere and are less affected by the contact surface.

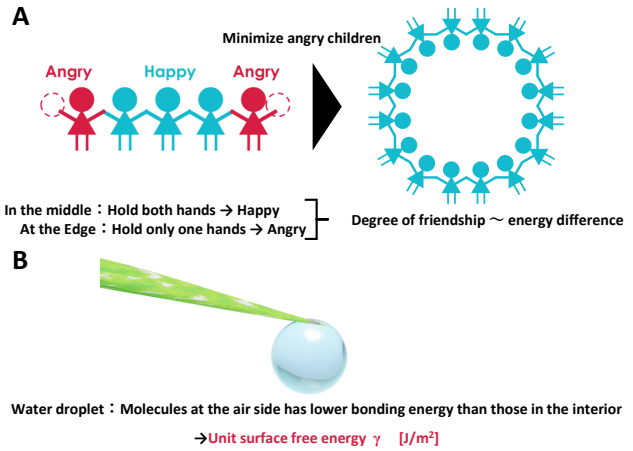

C

Liquid	Hexane	Glycerol	Water	Mercury
γ [mJ/m²]	18.4	63	72	480
Molecular interaction	van der Waals	＋Hydrogen bond		＋metallic bond

Fig. 1. (A) Example to understand the surface free energy. A group of children stand side by side, holding hands. The children at the ends and those in the middle are unequal because they hold different numbers of hands. The closer the friendship between the children is, the greater the difference in mood becomes. To eliminate this inequality, the children at the ends can join hands to form a circle. (B) A drop of water on a leaf causes unfairness in the number of bonds between the water molecules inside and at the air boundary. The energy difference between these molecules is the surface free energy. To minimize the number of surface molecules, the droplet becomes spherical. (C) Examples of liquid species and their surface free energy. The magnitude of the surface free energy is determined by the strength of the interaction between the molecules (degree of friendship).

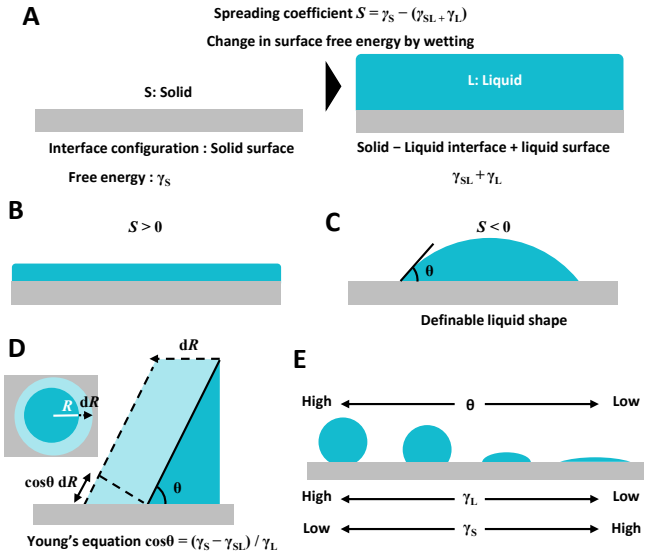

Fig. 2. (A) Spreading coefficient S: change in surface free energy when wetting a solid surface. (B) Complete wetting of the liquid when $S > 0$. (C) Incomplete wetting of the liquid when $S < 0$. The contact angle θ quantifies the droplet shape. (D) Young's equation: the relationship between the droplet's static shape and surface free energy. (E) Relationship between contact angle and surface free energy.

2.2 Droplet shape

The energy difference between molecules occurs not only at the liquid surface (interface with air) but at all interfaces. For example, tone can easily imagine the existence of an energy difference between the interior of water and oil as well as at the water–oil interface. In other words, free energy exists at the surfaces and interfaces of different materials. Thus, the surface free energy can be applied to all surfaces and interfaces, and the surface (interfacial) free energy γ is generally expressed (in subscript form) as the first letter of the English name of the state of the material that forms the interface. Therefore, the surface free energy of solids and liquids as well as the interfacial free energy of the solid–liquid interface are expressed as γ_S, γ_L, and γ_{SL}, respectively. Next, we consider a system in which a solid surface is completely wetted by a liquid (Fig. 1A). In this case, the surface of the system is the solid surface before wetting, and the free energy is expressed as γ_S. After wetting, the solid surface disappears, and a solid–liquid interface and liquid surface form in its place. Therefore, the free energy of the system is expressed as $\gamma_{SL} + \gamma_L$. The change in surface free energy due to wetting, $S = \gamma_S - (\gamma_{SL} + \gamma_L)$, is represented by the spreading coefficient.

When $S > 0$, the energy of the system decreases as the solid surface becomes wet, and the liquid disperses. Meanwhile, when $S < 0$, the liquid cannot completely wet the solid surface and remains as a droplet on the solid surface. Thus, the shape of the droplet can be defined by the contact angle θ, which is the angle between the solid–liquid interface and liquid surface.

Next, we consider the relationship between θ and the surface free energy. As shown in Fig. 2D, consider a change in free energy dE when the solid–liquid interface is displaced by dR in the wetting direction. By denoting R as the contact radius of the droplet, the area of the liquid wetting the surface is $2\pi R\,dR$, and the surface area of the liquid increases by $2\pi R\cos\theta\,dR$. Here, $dE = 2\pi R(\gamma_{SL} - \gamma_S)\,dR + 2\pi R\gamma_L\cos\theta\,dR$. When the droplet is stationary, $dE = 0$. Therefore, the Young's equation can be written in as follows [6]:

$$\cos\theta = \frac{\gamma_S - \gamma_{SL}}{\gamma_L}$$

Here, substituting $S = \gamma_S - (\gamma_{SL} + \gamma_L)$ into Young's equation yields $S = \gamma_L(-1 + \cos\theta)$. By considering $\cos\theta < 1$, the droplet shape can only be defined when $S < 0$.

Figure 2E shows the droplet shape under different θ. At larger θ, the droplet become more spherical, and a constant volume resulted in a smaller apparent contact area with the solid. Therefore, in many cases, the adhesive force of the liquid was assumed to decrease as θ increased, thereby increasing the hydrophobicity/oleophobicity. Based on Young's equation, θ increases as the liquid surface free energy and solid–liquid interfacial energy increase, and as the solid surface free energy decreases. For example, the θ of a water droplet on fluororesin is larger than that on a glass substrate. Even on fluororesin, the θ of vegetable oil is smaller than that of water.

2.3 Surface tension and capillary force

In Sect. 2.1, we explained that the surface free energy is the energy per unit area, which increases with the water droplet surface area, and that it is expressed in units of J/m^2. Notably, $J/m^2 = N/m$, and the surface free energy has the same units of tension as the spring constant. In other words, analogous to the force that attempts to contract a rubber band when stretched being characterized by a spring constant, surface tension acts similarly on water droplets to reduce their surface

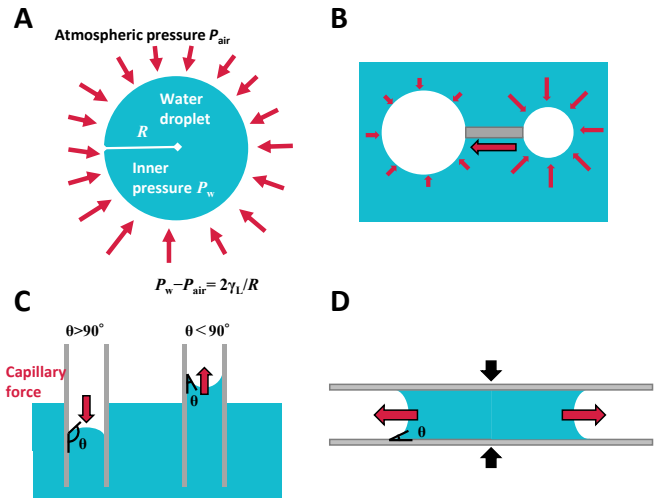

Fig. 3. (A) Laplace pressure: increase in internal pressure of a droplet due to surface tension. (B) Bubble coalescence underwater owing to Ostwald ripening. (C) Ascend and descend of the liquid level due to capillary phenomenon. (D) Capillary adhesion phenomenon.

area and is used as a vector quantity of surface free energy. Here, we consider the difference between a rubber band and water droplet. Even when a water droplet becomes spherical (Fig. 1B) and its surface area is minimized, tension will continuously reduce the surface area. This results in the internal pressure P_w of the water droplet increasing more than the atmospheric pressure P_{air} until it balances with the surface tension (Fig. 3A). The pressure increase $P_w - P_{air}$ at this time is known as the Laplace pressure. Next, we examine the relationship between the Laplace pressure and surface free energy. When a water droplet with radius R expands by dR, its volume and surface area increase by $4\pi R^2\,dR$ and $8\pi R\,dR$; therefore, its energy change dE is expressed as $dE = -(P_w - P_{air})(4\pi R^2\,dR) + \gamma_L(8\pi R\,dR)$. By considering a static state ($dE = 0$), we obtain Laplace's equation as follows: $P_w - P_{air} = 2\gamma/R$. Here, the surface-tension direction is determined by the surface curvature $2/R$ of the liquid. For example, a comparison of a bubble in water with a droplet in air shows that the curvature of the water surface is reversed, which implies that the surface-tension is reversed as well. Consequently, the bubble pressure is greater than the water pressure. This internal pressure increases as the bubble size decreases. Therefore, when connecting two bubbles of different sizes by a capillary tube, as shown in Fig. 3B, the smaller bubble is drawn into the larger bubble and merges with it, which is a phenomenon known as Ostwald ripening. This is caused by the macroscopic force of the bubbles traversing through the capillary tube due to surface tension, and this force is known as the capillary force. In this case, the capillary force is obtained by scaling the surface tension (N/m) by the length (m) of the contact line among the three phases, i.e., the water, bubble, and solid (capillary tube) phases. The capillary force acts similarly in any system with three phases in contact.

Thus, a question arises: Can the direction of the capillary force be controlled by the material? Figure 3C shows that the immersion of a capillary in liquid causes the liquid level to ascend and descend, which is known as the capillary phenomenon. When the inner wall of the capillary, the liquid, and the gas form a three-phase interface, the surface curvature of the liquid changes depending on θ. For example, in cases where the liquid phase is water, a hydrophobic capillary ($\theta > 90°$) will cause the liquid level to exhibit an upward convex shape, whereas the capillary force causes the water level to descend (buoyancy and capillary forces are in balance). Meanwhile, a hydrophilic capillary ($\theta < 90°$) causes the water level to ascend to a height where gravity and capillary forces are in balance.

Capillary adhesion is a typical example of capillary force (Fig. 3D). The phenomenon of wet hair clumping together or wetted sheets adhering together is caused by water droplets stretching in the lateral direction via capillary force, thus resulting in the action of stress bringing the solid surfaces closer together.

3. Surface structure and wetting phenomenon

3.1 Wenzel model [7] and Cassie–Baxter model [8]

In Sect. 2, we explained the effects of droplets and solid materials on wetting phenomena. Next, we explain the effects of the surface shape of a solid on wetting. Various models have been developed for this topic; however, the two most commonly used models in modern studies are the Wenzel and Cassie–Baxter models, which can be explained via classical theory. In the Wenzel model, we consider a Wenzel state of liquid penetrating and adhering to a surface with surface roughness r (ratio of surface area of rough surface to that of flat surface) without any gaps (Fig. 4A). Here, we consider the apparent contact angle θ_w, which changes depending on surface roughness, using the same derivation process as that for Young's equation. As shown in Fig. 4B, we consider the change in free energy when the solid–liquid interface is displaced by dR in the wetting direction. By denoting the contact radius of the droplet as R, the area wetted by the liquid on the substrate is expressed as $r \times 2\pi R\,dR$, and the surface area of the liquid increases by $2\pi R\cos\theta_w\,dR$. The change in free energy at this time is expressed as $dE = 2\pi R(\gamma_{SL} - \gamma_S)r\,dR + 2\pi R\gamma_L\cos\theta_w\,dR$. Combining the fact that $dE = 0$ when the

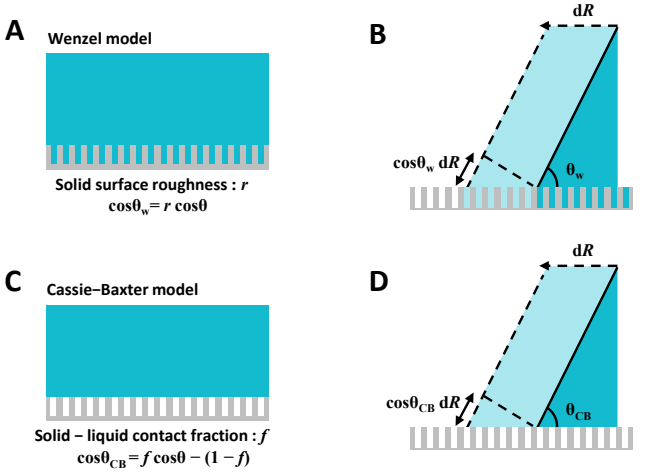

Fig. 4. (A) Wenzel model: state in which liquid on the rough surface fills the rough surface without gaps. (B) Relationship between rough surface topography and surface free energy change in the Wenzel model. (C) Cassie–Baxter model: state in which an air layer is entrapped in the gap between the rough surface and the liquid. (D) Relationship between rough surface topography and surface free energy change in the Cassie–Baxter model.

droplet is static and Young's equation $\cos\theta = (\gamma_S - \gamma_{SL})/\gamma_L$, we obtain Wenzel's equation as follows:

$$\cos\theta_w = r\cos\theta,$$

where θ is the contact angle determined by the material of the solid and liquid type, with $\theta_w > \theta$ when $\theta > 90°$ and $\theta_w < \theta$ when $\theta < 90°$. Unlike the case of a flat surface, in the Wenzel state, the contact angle becomes larger, and the apparent contact area between the droplet and rough surface decreases (Fig. 2E). However, the actual contact area of the solid–liquid interface increases by r; thus, the adhesive force of the droplet does not decrease [9].

Meanwhile, the Cassie–Baxter model primarily explains the apparent contact angle θ_{CB} in the Cassie–Baxter state where an air layer is included between the liquid and rough surface, and the liquid is left stationary (Fig. 4C). The contact ratio of the air layer is expressed as $1 - f$, where f is the contact ratio of the solid–liquid surface between the liquid and rough surface. As in the example, we consider the change in free energy when the solid–liquid interface is displaced in the wetting direction by dR, as shown in Fig. 4D. By denoting the contact radius of the droplet as R, he area where the liquid wets the substrate is $2\pi Rf\,dR$, and the surface area of the liquid increases by $2\pi R\cos\theta_{CB}\,dR + 2\pi R(1-f)\,dR$. The change in free energy at this time is expressed as $dE = 2\pi R(\gamma_{SL} - \gamma_S)f\,dR + 2\pi R\gamma_L\cos\theta_{CB}\,dx + 2\pi R\gamma_L\,dR(1-f)$. Combining the fact that $dE = 0$ when the droplet is static and Young's equation $\cos\theta = (\gamma_S - \gamma_{SL})/\gamma_L$, we obtain Cassie–Baxter's equation as follows:

$$\cos\theta_{CB} = f\cos\theta - (1-f),$$

where a smaller f results in a larger apparent contact angle θ_{CB} and a smaller apparent contact area between the droplet and rough surface (Fig. 2E) [9]. The actual contact area of the solid–liquid interface is the apparent contact area multiplied by f. This results in a liquid adhesive force that is significantly smaller than that of a flat surface or rough surface in the Wenzel state. In particular, the droplet rolls off the solid surface when the contact angle of a droplet exceeds 150° in the Cassie–Baxter state. This phenomenon is known as superhydrophobicity when the droplet is water, and superoleophobicity when the droplet is vegetable oil or an organic solvent.

3.2 Superhydrophobic surfaces and liquid marbles

How do we design a surface structure that maintains the Cassie–Baxter state? Here, we once again consider the example of capillary-tube action (Fig. 5A). When we immerse a hydrophobic ($\theta > 90°$, i.e., $\cos\theta < 0$) capillary tube in water, the capillary force F_{cap} causes the water level inside the capillary tube to be lower than the water surface, which balances with the hydrostatic pressure (buoyancy). If we set the inner diameter of the capillary tube to $2r$, then the capillary force can be expressed by scaling the surface tension by the contact-line length as $F_{cap} = 2\pi r(\gamma_{SL} - \gamma_S) = -2\pi r\gamma_L\cos\theta$. The capillary force per unit area (i.e., water-resistance pressure) is expressed as $F_{cap}/\pi r^2 = -2\gamma_L\cos\theta/r$, which implies that a thinner capillary tube results in a greater water-resistance pressure per unit area. If we set the decrease in the water level as h, then the balance between the hydrostatic pressure (buoyancy) and water-resistance pressure (capillary force) yields the relation $-2\gamma_L\cos\theta/r \approx \rho gh$ (ρ: water density, g: gravitational acceleration), with a thinner capillary tube resulting in a greater decrease in the water level. Additionally, the stability of the Cassie–Baxter state is determined by the balance between the water-resistance and hydrostatic pressures.

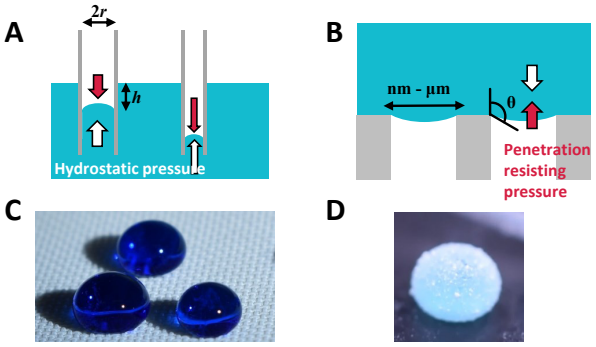

Fig. 5. (A) Relationship between the width of the capillary tube and descent water level in the capillary phenomenon. (B) A water droplet on a hydrophobic lattice structured surface. (C) Water droplets on the superhydrophobic nano-coated fabric. (D) Non-wetting droplets: liquid marble formed by adsorption of superhydrophobic nanoparticles on water droplet surface.

Next, we consider the state in which a water droplet is deposited on a fine hydrophobic lattice structure, as shown in Fig. 5B. Here, the hydrostatic pressure resulting from gravitational force exerting on the water droplet can be obtained by replacing the decrease in the water level h in Fig. 5A with the thickness of the water droplet. The thickness of the water droplet is limited by gravity, and its maximum value is approximately $2(\gamma_L/\rho g)^{0.5}$, where $L_c = (\gamma_L/\rho g)^{0.5}$ is known as the capillary length, which is approximately 2.8 mm for water. In other words, maintaining the Cassie–Baxter state should result in a water-pressure resistance that is significantly greater than the hydrostatic pressure, which would be satisfied if $-2\gamma_L\cos\theta/r \gg 2\rho gL_c$ or $L_c \gg r/(-\cos\theta)$. Qualitatively, the stability of the Cassie–Baxter state can be improved using a fine uneven structure ($r \to$ small) and a material with high hydrophobicity ($\theta \to$ large). When using actual hydrophobic surfaces, the hydrodynamic pressure arising from the collision of water droplets is applied; therefore, a higher water-pressure resistance is favored.

Figure 5C shows the use of nanoparticles modified with hydrocarbon groups to form a nanometer-scale hydrophobic uneven structure on a substrate (Fiber), which achieves the Cassie–Baxter state. Meanwhile, Fig. 5D shows the adsorption of hydrophobic nanoparticles to the water droplet surface to achieve the Cassie–Baxter state. The former is known as a superhydrophobic surface, whereas the latter hydrophobic water droplet is known as a liquid marble [10]. In both cases, the water droplet rolls on the substrate surface.

However, the fine uneven structure is fragile and easily destroyed by mechanical stimuli. Therefore, various approaches have been considered for creating a superhydrophobic surface with high mechanical durability [11]. Minute water droplets such as condensation water and mist can occupy the gap between the uneven structures, thus inducing the Wenzel state and increasing the adhesion force of water. Surface design methods for repelling minute water droplets have been devised in recent years [12].

3.3 Re-entrant shape and superoleophobic surface

When the target liquid is water, surface modification with

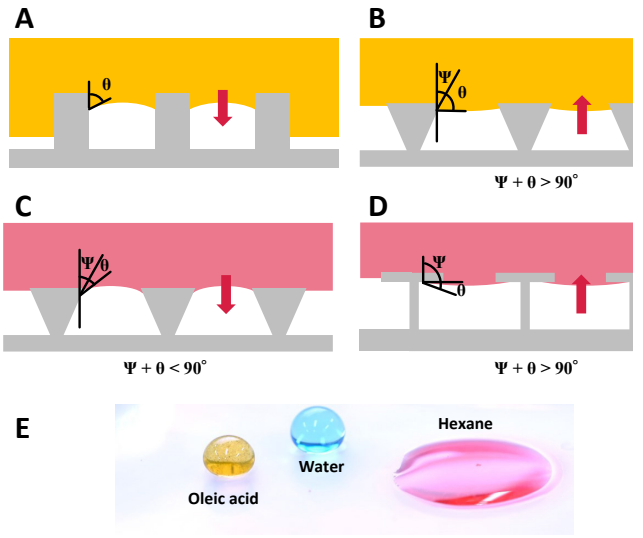

Fig. 6. (A) Oleic acid on a lattice structure. (B) Oleic acid on an inverted tapered structure. (C) Hexane on the inverted tapered structure. (D) Hexane on a T-shaped structure. (E) Drops of water, oleic acid, and hexane on a glass substrate with the inverted tapered nanostructure.

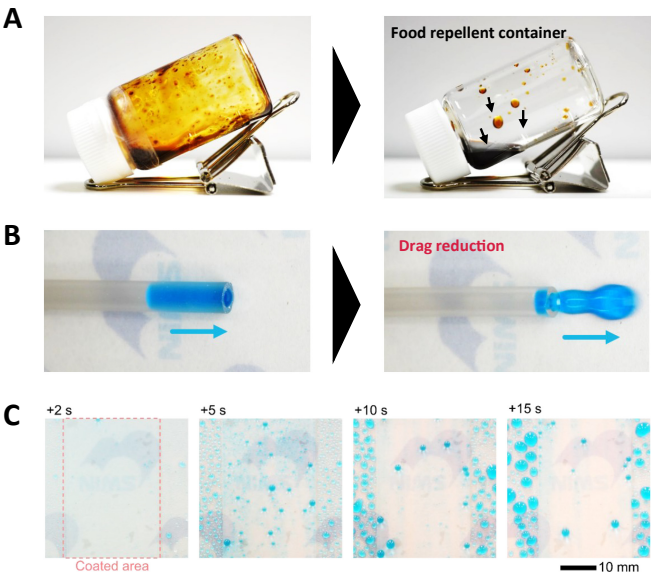

Fig. 7. (A) Repellency of BBQ sauce in the oleophobic glass container. (B) Enhanced water transportation inside the silicone tubes with water-repellent inner walls. (C) The mist-repellent coating on the glass substrate. (B and C) Reproduced with permission from Ref. 14. © 2022 Wiley-VCH GmbH.

hydrocarbons or fluorocarbon groups can achieve a surface with $\theta > 90°$. However, no material can afford a surface with $\theta > 90°$ for liquids with low surface energy, such as vegetable oils (e.g., oleic acid) and organic solvents (e.g., hexane). Therefore, as shown in Fig. 6A, when depositing oleic acid onto a hydrophobic lattice structure (assuming $\theta = 60°$), capillary force acts in the direction in which the liquid penetrates the substrate, and the substrate transitions into the Wenzel state. Maintaining the Cassie–Baxter state for liquids with $\theta < 90°$ requires a specific surface structure.

A re-entrant structure (rat-guard structure) is formed on the superoleophobic surface [13]. Figure 6B shows oleic acid placed on an inverted tapered structure that tapers toward the bottom of the substrate. Here, the shape of the re-entrant structure is defined by the angle Ψ of the tapered structure. Thus, the condition for the capillary force to resist the liquid pressure is $\Psi + \theta > 90°$, since the gas–liquid interface must form a downward convex structure, as shown in Fig. 6B. This enables the Cassie-Baxter state to be maintained even for liquids with $\theta < 90°$. However, even if the material is superoleophobic, the contact angle varies depending on the type of organic solvent or oil. For example, applying hexane (assuming $\theta = 20°$) to an inverted tapered structure as shown in Fig. 6C results in a Wenzel transition when $\Psi + \theta < 90°$. However, depositing hexane onto a T-shaped structure with $\Psi = 90°$ as shown in Fig. 6D allows for the Cassie–Baxter state to be maintained. Achieving a re-entrant structure on a fine scale is ideal for reducing the contact area between the liquid and structure. Similarly, modification with fluorocarbon groups is ideal for achieving $S < 0$ for oils and organic solvents.

The results above show that establishing a process technology for forming re-entrant structures over a large area and the use of fluorine materials, which pose cost and environmental issues, are challenging. Furthermore, the development of surfaces that repel liquids with lower surface energy is necessitated. Figure 6E shows a surface modified with fluorocarbon group-modified nanoparticles into an inverse tapered structure. As shown, the structure exhibits superhydrophobicity and superoleophobicity against water and oleic acid, although hexane droplets wetted the surface and spread on it. As with superhydrophobic surfaces, these surfaces present issues such as mechanical durability and loss of repellency against microdroplets.

4. Hydro- and oleophobic surfaces and their application to droplet-transport technology

Next, we introduce hydrophobic/oleophobic-surface application examples along with our recent results. Hydro- and oleophobic surfaces can reduce the adhesion loss of droplets to almost zero, thus enabling highly efficient liquid transport. For example, when retrieving food from a container, some of the food remains on the container due to wetness. This residue causes food waste, bacterial growth, and high cleaning costs. Figure 7A shows that using a glass container that underwent oleophobic treatment allows one to pour out the BBQ sauce completely without any adhesion loss. Liquid repellency is not limited to food, and this technology may be able to eliminate the adhesion loss of liquids in diverse environments.

Meanwhile, the lack of water adhesion would significantly benefit the industrial field. For example, metal corrosion due to salt water, power-line freezing, and reduced efficiency due to condensation on heat exchangers are caused by water adhesion. Researchers have attempted to solve these issues by applying hydrophobic surface treatments. Figure 7B shows that flow resistance can be reduced via hydrophobic treatment. Subjecting hydrophobic treatment to the inner walls of a silicone tube resulted in a 50-fold increase in the water-delivery speed [14]. However, the wetting phenomenon changed depending on the water-droplet size and contact state; therefore, surface design methods must be further investigated. Figure 7C shows a surface that can slide mist, and this surface adopts a design that promotes the coalescence of mist particles and the growth of water droplets to facilitate

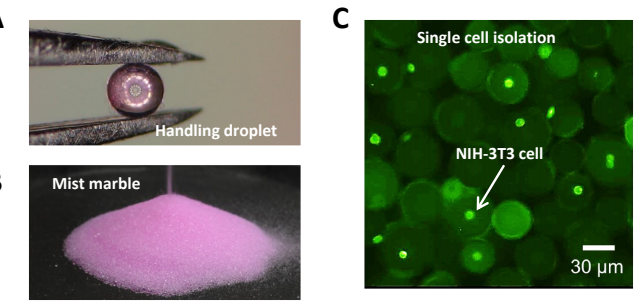

Fig. 8. (A) Liquid marble technology enabled the droplet handling. (B) Powder-like fluidity of micro-liquid marbles. (C) Cell isolation using micro-liquid Marbles. (A–C) Reproduced with permission from Ref. 16. © 2023 Wiley-VCH GmbH.

their sliding [14]. Recently, we published an open-access review that summarizes the applications of droplet-transport technology and surface design methods; interested readers can refer to this paper [5].

Finally, we introduce an application example of non-wetting droplet liquid marbles. The liquid marble introduced in Sect. 3.2 forms a superhydro (oleo) phobic structure on a water (oil) droplet surface, thereby eliminating contact with the substrate. This allows the liquid marble to be regarded as a soft solid material (Fig. 8A) that can be prepared or transported remotely by external stimuli. Changing the liquid type to a reagent, indicator, or cell suspension is expected to enable laboratory-in-a-marble applications, which allow chemical reactions, sensing, and cell-culture experiments at droplet sizes. Readers should refer to our open-access review for more information [15]. Most liquid marbles are prepared as droplets measuring 2–3 mm; however, we have successfully prepared liquid marbles of micrometer size (mist marbles) [16]. A group of micro liquid marbles behaves similarly to dry powder, despite having a moisture content of approximately 99% (Fig. 8B). We successfully trapped individual cells inside liquid marbles by forming a cell suspension in the internal liquid of the liquid marbles and designing the size of the liquid marble to be equivalent to that of the cells (i.e., approximately 10 μm) (Fig. 8C). The liquid marbles encapsulating the cell forms a superhydrophobic structure on their surface; therefore, they do not adhere to each other and maintain a dry powder-like state. Therefore, we name this a "drycell" and attempt to apply it as a cell-isolation tool for single-cell analysis techniques.

5. Summary

In this paper, we explained the basic theory of wetting phenomena and superhydrophobic/superoleophobic surface design methods. Owing to space constraints, we have limited our explanation to systems of droplets in air. Nonetheless, the theory can be extended to systems that include bubbles in water and immiscible liquid–liquid interfaces such as water and oil. Recently, researchers have actively investigated surfaces that reduce the friction of liquids by achieving a flat surface on a molecular scale, thereby allowing them to "slide" [17,18]. The combinations of target liquids and surface structures are numerous, and many challenges remain for their practical application, such as durability, manufacturing process, and costs. Furthermore, their application scope is extremely broad; therefore, new demand may arise as other fields continue to develop. Readers who are interested in this field should begin studying common wetting phenomena.

References

[1] P. G. Gennes, F. Brochard-Wyart, and D. Quéré, *Capillarity and Wetting Phenomena* (Springer, 2004).
[2] H.-J. Butt, K. Graf, and M. Kappl, *Physics and Chemistry of Interfaces* (Wiley-VCH, 2013).
[3] T. Onda, S. Shibuichi, N. Satoh, and K. Tsujii, Langmuir **12**, 2125 (1996).
[4] R. Wang, K. Hashimoto, and A. Fujishima, Nature **388**, 431 (1997).
[5] M. Tenjimbayashi and K. Manabe, Sci. Technol. Adv. Mater. **23**, 473 (2022).
[6] T. Young, Philos. Trans. R. Soc. London **95**, 65 (1805).
[7] R. N. Wenzel, Ind. Eng. Chem. **28**, 988 (1936).
[8] A. B. D. Cassie and S. Baxter, Trans. Faraday Soc. **40**, 546 (1944).
[9] A. Lafuma and D. Quéré, Nat. Mater. **2**, 457 (2003).
[10] P. Aussillous and D. Quéré, Nature **411**, 924 (2001).
[11] T. Verho, C. Bower, P. Andrew, S. Franssila, O. Ikkala, and R. H. A. Ras, Adv. Mater. **23**, 673 (2011).
[12] T. Mouterde, G. Lehoucq, S. Xavier, A. Checco, C. T. Black, A. Rahman, T. Midavaine, C. Clanet, and D. Quéré, Nat. Mater. **16**, 658 (2017).
[13] A. Tuteja, W. Choi, J. M. Mabry, G. H. McKinley, and R. E. Cohen, Proc. Natl. Acad. Sci. U.S.A. **105**, 18200 (2008).
[14] M. Tenjimbayashi, G. Hayase, T. Hiroi, and T. Ueki, Adv. Mater. Interfaces **9**, 2200497 (2022).
[15] M. Tenjimbayashi, T. Mouterde, P. K. Roy, and K. Uto, Nanoscale **15**, 18980 (2023).
[16] M. Tenjimbayashi, S. Yamamoto, and K. Uto, Adv. Mater. **35**, 2300486 (2023).
[17] L. Chen, S. Huang, R. H. A. Ras, and X. Tian, Nat. Rev. Chem. **7**, 123 (2023).
[18] T.-S. Wong, S. H. Kang, S. K. Y. Tang, E. J. Smythe, B. D. Hatton, A. Grinthal, and J. Aizenberg, Nature **477**, 443 (2011).

Profile

Mizuki Tenjimbayashi is an independent researcher at the Research Center for Materials Nanoarchitectonics (MANA), National Institute for Materials Science (NIMS). He received his Ph.D. from Keio University in 2017 and joined NIMS in 2018 as a postdoctoral fellow. In 2019, he started his independent research career. He is concurrently working as a visiting professor at Chuo University.